Australian Government
Department of Defence
Defence Science and
Technology Organisation

# Gamma Imaging using Rotational Modulation Collimation

***M. Roberts M. Kocan, A. Eleftherakis, D. Marinaro and A. Meehan***

**Land Division**

**Defence Science and Technology Organisation**

**DSTO–TR–2946**

## ABSTRACT

This report describes measurements undertaken at the DSTO radiation laboratory to characterise the performance of two rotating modulation collimator (RMC) gamma imagers built by DSTO. The ability of these devices to image shielded and unshielded Co-60 and Cs-137 sources is demonstrated. A discussion of the characteristics of this and other gamma imaging techniques and their application in a Defence context is included.

**APPROVED FOR PUBLIC RELEASE**

*Published by*

*DSTO Defence Science and Technology Organisation*
*506 Lorimer St,*
*Fishermans Bend, Victoria 3207, Australia*

*Telephone: 1300 333 362*
*Facsimile: (03) 9626 7999*


*AR No. 015-881*
*January 2014*

***APPROVED FOR PUBLIC RELEASE***

# Gamma Imaging using Rotational Modulation Collimation

## Executive Summary

This report describes the development at DSTO of two prototype gamma imaging devices. These devices use a technique called rotational modulation collimation to generate an image of the gamma radiation field. Previous studies undertaken by DSTO, and in collaboration with international partners, have identified imaging as a way to significantly improve the current radiological source search capability of Defence and other Government agencies. As well as increased detection sensitivity, imaging provides information on source location which reduces search time and the radiation exposure to personnel.

A summary of gamma imaging techniques is included in this report in addition to a description of the two imaging devices built at DSTO. A series of experimental measurements demonstrated that the imagers were able to detect and image gamma sources under a variety of source shielding conditions. These included placing the sources in lead shielded transport containers and behind a 0.5 m thick masonry wall.

Rotational modulation collimator (RMC) detectors are rugged and relatively inexpensive and may provide a practical capability for radiological source search problems. The lessons learned from the construction of the imaging prototypes are being incorporated into a field-able prototype that will be used to demonstrate this capability to Defence.

Data from the gamma imaging experiments will be used as a test bed for developing a sophisticated simulation capability at DSTO based on the Geant4 radiation simulation package.

THIS PAGE IS INTENTIONALLY BLANK

# Authors

**Michael Roberts**
*Land Division*

Michael Roberts gained a PhD in high energy astrophysics in 1994 from the University of Adelaide. He worked as an astrophysicist in the United Kingdom, Japan and the United States before joining DSTO in 2007 as a Defence Scientist. His current research areas include radiation simulation and detection and mathematical modelling of equipment for protection against airborne hazardous agents.

**Martin Kocan**
*Land Division*

Martin Kocan obtained his PhD from the University of Aachen, Germany in 2003 and subsequently worked as a research scientist at the University of Goettingen, Germany, at the University of Western Australia and at Solar Systems Pty Ltd. Martin has been working in the Land Division at DSTO since 2010.

**Arthur Eleftherakis**
*Land Division*

Arthur Eleftherakis is a Defence Scientist working in Land Division who has a B.Sc. from the University of Melbourne and B.Sc.(Hons) from Monash University. Arthur joined DSTO in 1990 and gained his PhD in Safety Science from the University of NSW in 1999. His interests are in the areas of radiological defence and radiation instrumentation.

**Damian Marinaro**
*Land Division*

Damian Marinaro is a Defence Scientist working in the Land Division of DSTO. From Jan 2011 to Dec 2012 Damian held the post of Senior Special Operations Science & Technology Adviser embedded within the Special Operations Engineer Regiment, and concurrently held a Visiting Scientist position at the Australian Nuclear Science & Technology Organisation. His research interests are broadly in the area of nuclear and radiological defence, including in particular standoff detection of radiation. He received his PhD in Physics from the University of Wollongong in 2003 and is a member of the Australian Institute of Physics and the IEEE.

**Alaster Meehan**
*Land Division*

Alaster Meehan graduated from Melbourne University in 2003 with a double degree in Science (Physics) and Computer Engineering. In 2005, he commenced a PhD in adaptive optics at Melbourne University, whilst working at Iatia developing ophthalmic instrumentation. In 2010 Alaster started working as a contractor for DSTO working on radiation simulation, disease modelling and visual signatures.

# Contents



# Appendices

THIS PAGE IS INTENTIONALLY BLANK

# 1 Introduction

The risks posed to human health and to the disruption of society from radioactive material that is misused - either through deliberate malicious actions or unintentional accidents - is well recognised (see for example [1]). In order to avoid the potentially disastrous consequences of the employment of a Radioactive Dispersal Device (RDD) by a terrorist organisation, the Australian Government and the Australian Defence Force have maintained a capability to search for and locate radioactive material that has been either confirmed to be or suspected of being lost, stolen or diverted.

At present, the principal technique for searching for radiation sources is through the use of vehicle-mounted or hand-held radiation survey equipment. This involves a time-consuming process of sweeping through an area while looking for a change in the intensity of radiation as indicated on the detection instrument. At DSTO we have a long standing interest in radiation detection, including using non-imaging gamma detectors to search for radiological sources. As part of this research program a multi-source field trial was undertaken by DSTO to investigate source search methodologies. Analysis of results from this trial was consistent with previous experience for both human directed and computerised search strategies. If the hazard is relatively simple, such as a single strong source in an uncluttered environment, then both human operators and computerised search algorithms can reliably find the source [2, 3, 4]. The search is much more difficult if the source or environment is complex. The source may be weak or heavily shielded making it hard to distinguish from the spatially variable background and multiple or distributed sources also complicate a search. If the environment is complex, attenuating objects such as buildings, cars or trees will change the detected signal in ways that can't be predicted without detailed modelling.

The use of gamma imaging technology was identified in a DSTO review of the Radiological Defence System as an alternative search method which has the potential to significantly increase the speed and efficiency of source search and localisation [5]. Instead of requiring one or more people to sweep through an area looking for a variation in the radiation signal, a gamma imager operated by a single person would provide a visual representation of the direction and variation in intensity of gamma radiation within a field of view. When overlayed onto a photographic image of the scene, the specific location of any significant sources of radiation would be rapidly distinguishable.

The benefits of imaging over traditional survey detection have recently been highlighted in work undertaken by the International Task Force - 53 (ITF-53), a team of radiation experts from Australia, Canada, the United Kingdom and the United States, instituted under the auspices of the Chemical, Biological and Radiological Memorandum of Understanding (CBR MOU). ITF-53 analysed the probability of detection for various radiation sources using several detection scenarios, given an average background radiation signal with a typical statistical variation and against various shielding thicknesses. The results of the analysis [6] determined that the application of even crude imaging with a coarse spatial resolution allowed significant improvements in detection probabilities over traditional gamma detection, especially when the radiation source was shielded.

Within DSTO the gamma imaging program will also be used to facilitate the development of a radiation simulation capability based on the Geant4 software package [7].

# 2 Gamma imaging techniques

Various techniques for gamma imaging have been developed over the decades, mainly for applications in astronomy and medical imaging [8, 9], but also proposed for use in nuclear reactor decommissioning and nuclear arms verification [10].

Gamma imaging techniques are generally categorised according to the basic underlying physical principle of operation. The following sections give a brief overview of imaging techniques that are of relevance to national security applications.

## 2.1 Compton imaging

Compton scattering is a specific interaction mechanism between a gamma photon and an atomic electron, in which there is a partial transfer of energy to the electron and a resulting deflection of the photon. The photon scatters at an angle that depends on the magnitude of the energy transferred. Thus, by measuring the angle of scatter of the photon and the energy involved in two or more interactions, the trajectory of the photon can be reconstructed as a cone of possible arrival directions. Overlaying multiple trajectory cones over many gamma photon interactions reveals the source position, and this forms the basis for the technique of Compton imaging [11]. Due to the need to measure multiple interactions of a single photon, a Compton imager requires at least two or more position-sensitive detection planes where the Compton scattering occurs and some imagers also require an additional detector plane that absorbs the remaining photon energy. Detection events must be measured in coincidence in order to attribute the events to a single photon, and so timing within the detector is critical. Thus a Compton imager is a relatively complex instrument.

## 2.2 Pinhole or parallel-hole collimation

The pinhole collimator imager consists of a position-sensitive gamma detector covered by a hollow cone made of a dense material (typically lead or tungsten) which has a small aperture at the apex. It works using the same principles as an optical pinhole camera, also magnifying and inverting the image as a pinhole camera does. The parallel-hole collimator extends multiple apertures along the length and breadth of the imaging plane. The array of parallel holes can improve sensitivity by allowing more photons to reach the detector, but at the expense of spatial resolution. The resolution and sensitivity of the pinhole imager are very dependent on the distance from the object to the camera, providing greater resolution for objects closer to the camera, but with decreased sensitivity [9]. The pinhole collimation imager is typically employed in small animal medical imaging or for medical imaging of specific human organs. The dependence on source-camera distance, the inherently low sensitivity and the low angular resolution mean that the pinhole imager is not ideal for national security applications. However, the principle of image reconstruction based on collimation has been extended to coded-aperture collimators and rotational modulation collimators.

## 2.3 Coded-aperture collimation

In a coded-aperture collimator, many collimation holes in the mask are arranged into a specific 2-dimensional pattern. A position-sensitive gamma detector behind the mask detects an image pattern which is then mathematically processed to reconstruct the gamma image. The combination thereby increases sensitivity over pinhole collimation without sacrificing spatial resolution [12]. The coded aperture imager is potentially limited by the degree of attenuation provided by the mask. For high-energy gamma rays, a significant thickness of material is needed in order to block a measurable portion of the radiation signal, resulting in a heavy mask. The mask thickness could be reduced to lessen the weight of the imager at the expense of the Signal-to-Noise Ratio in the reconstructed image [13].

## 2.4 Rotating modulation collimation

Rotating Modulation Collimators (RMCs) are constructed of two separate collimator grids over a bulk radiation detector, with each collimator consisting of parallel alternating gamma opaque slats and transparent slits. Rotation of the system about the collimator axis results in a modulation of the gamma count-rate from a point source over time, with the image of the point source reconstructed based on the structure of the modulation. RMCs have been in use in X-ray astronomy since the 1960's [14] and have been applied to high-energy gamma imaging in the last decade [15].

DSTO interest in the RMC gamma imaging technique is primarily due to its overall simplicity. RMC imagers are simple, rugged and relatively cheap to build. An RMC imager can provide excellent source reconstruction resolution over a wide field of view and the trade-off between field of view and resolution can be easily adjusted by altering the separation distance between the collimator grids. An RMC typically has few (even a single) large gamma detectors which are efficient at stopping and detecting gamma rays so an RMC can be efficient at relatively small size.

# 3 First prototype RMC

In figure 3.1 an image is shown of the first simple prototype of a rotating modulation collimator imager built at DSTO. This detector consists of the following components:

- Two Tungsten/Copper masks (75%/25% mass ratio) of thickness 1.2 cm
- Hollow aluminium tube mask support
- 2-inch NaI scintillation detector (BICRON G2; S/N:JJ-513)
- Readout electronics (CYPHER Model 5000; S/N:501133)

The rotation of the masks is achieved via a friction drive employing a stepper motor[1]. Data acquisition from the scintillation detector and the control of the stepper motor is performed using a custom made computer control program written in the Visual Basic programming language. The detector readout provides only a count-rate above a set

[1]Stepper drive MOT003 from PC Control Limited `http://www.pc-control.co.uk/stepper_motor.htm`

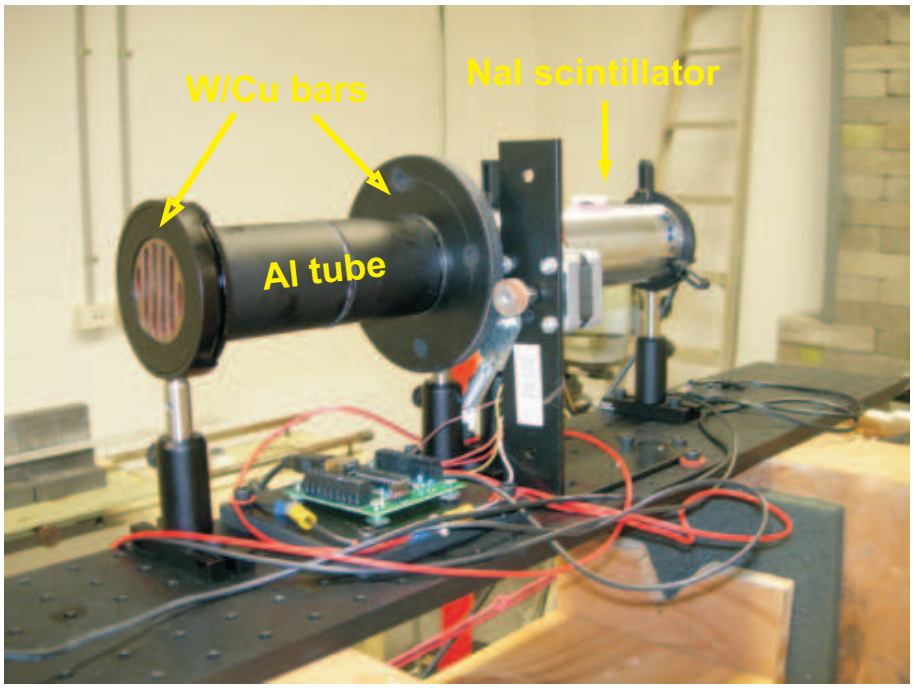


***Figure 3.1:*** *First prototype rotating modulation collimator gamma imager*

threshold level, so no detailed gamma energy spectrum is available.

The first version of the gamma imager was tested with Cs-137 (34.47 GBq) and Co-60 (0.74 GBq) radiation sources positioned at different distances and utilising different types of shielding materials (Appendix A). It was able to detect a measurable modulation signal through a variety of wood, metal, brick and lead shielding summarized in Table A2. Figures 3.2 and 3.3 show a selected set of collected modulation functions for radiation sources measured with a variety of source shielding. The typical measurement setup can be viewed in Appendix A in Figures A1 and A2 and the parameters of the gamma imager are summarised in Table A1.

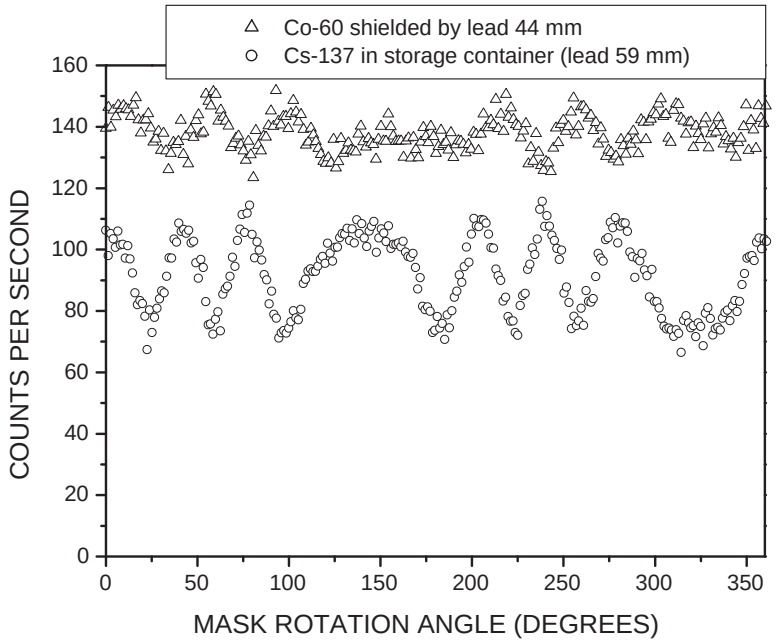


***Figure 3.2:*** *RMC version 1 imager modulation functions for measurements of Co-60 and Cs-137 radiation sources through shielding (see Table A2 for measurement details)*

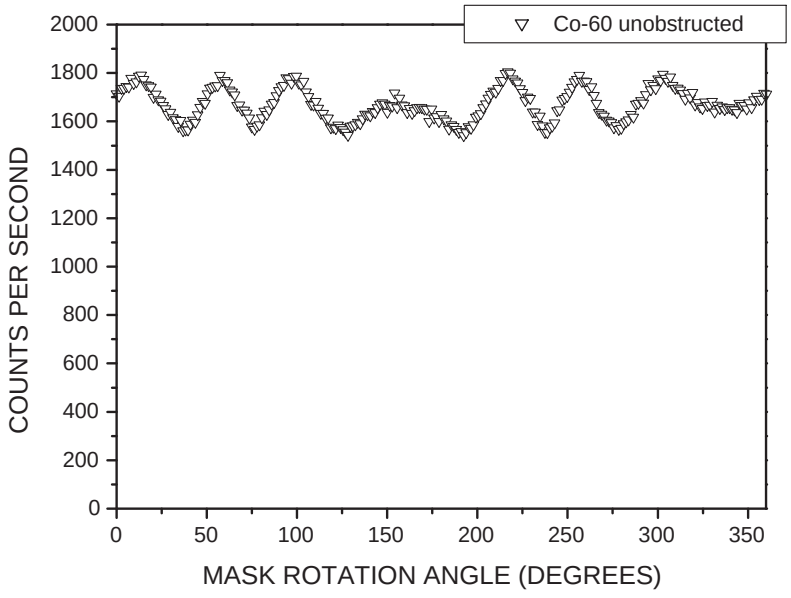


***Figure 3.3:*** *RMC version 1 imager modulation function for measuring an unobstructed C0-60 radiation source (see Table A2 for measurement details)*

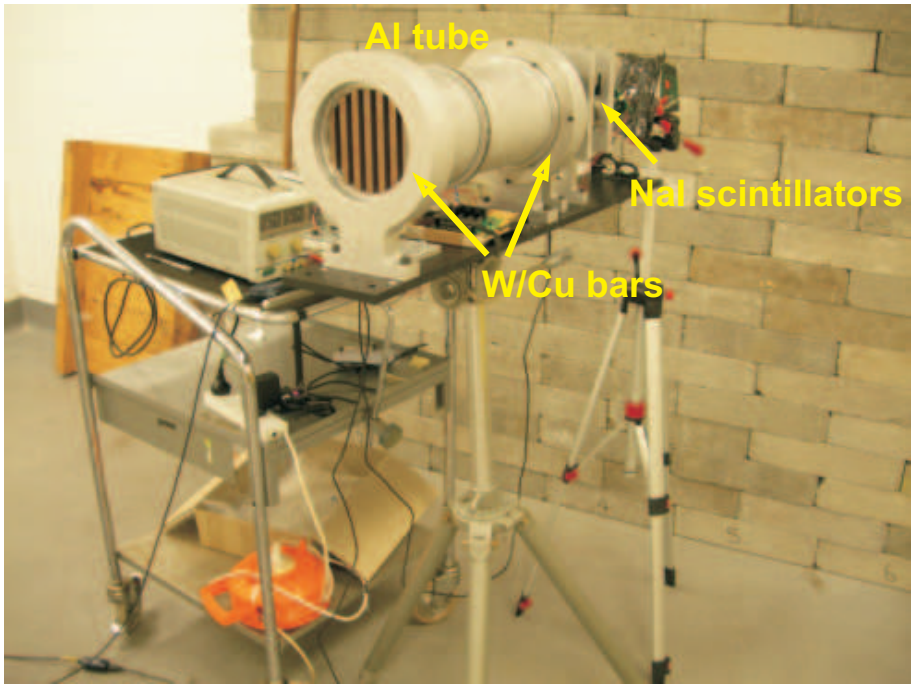


***Figure 4.1:*** *Second prototype RMC gamma imager*

# 4 Second prototype RMC imager

Figure 4.1 shows an image of the second prototype RMC imager developed at DSTO. The second version is approximately twice the size of the first and includes a number of design improvements that significantly improve its performance. The most important of these was to replace the single on-axis gamma detector with a cluster of three detectors. This detector pixelation increases the amount of information collected and reduces modulation function degeneracies for different source locations in the field of view. It also removes the unmodulated "dead area" that exists at the center of the rotation axis of the single detector RMC.

The second version of the RMC consists of the following components:
- Two Tungsten/Copper masks (75%/25% mass ratio) of thickness 1.9 cm
- Three 2x2-inch NaI scintillation detectors
  (Bridgeport instruments; Model: R2D-NaI-2; S/N:NaI-4560/4562/4563)[2]
- qMorpho (four channel Bridgeport Instruments DAQ card)

The rotation of the masks is achieved via a belt system driven by a stepper motor[3,4]. The measurement of the three detector signals and the control of the stepper motor are performed using a custom computer control program written in the C$^{++}$ programming language on an Ubuntu Linux operating system.

[2]Bridgeport instruments `http://www.bridgeportinstruments.com`
[3]MOT004 stepper motor from PC control limited `http://www.pc-control.co.uk`
[4]WTSMD-M stepper motor driver `http://www.weedtech.com`

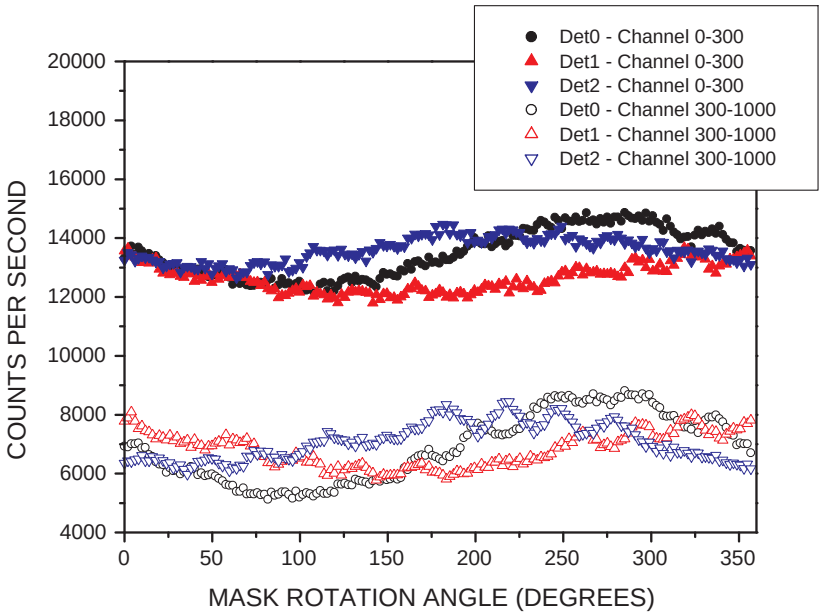


***Figure 4.2:*** *RMC gamma imager version 2 modulation function for a Co-60 (0.67 GBq) radiation source located on the rotation axis of the gamma imager at a distance of 7.3 m*

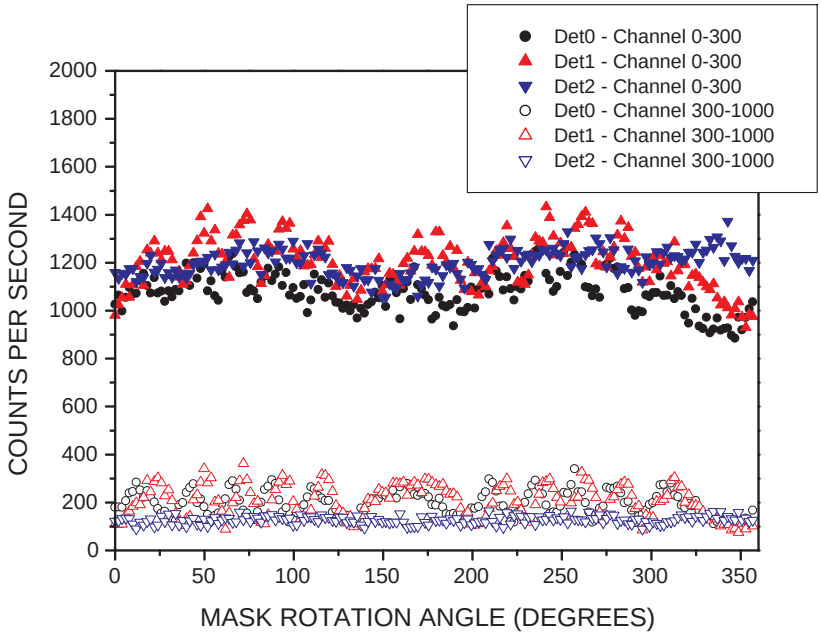


***Figure 4.3:*** *RMC imager version 2 modulation function for a Cs-137 (33.8 GBq) radiation source through a 0.5 m thick brick wall (source-RMC distance of 3.7 m)*

The performance of the second version RMC was tested with Cs-137 (33.8 GBq) and Co-60 (0.67 GBq) radiation sources positioned at different distances and with differing amounts of shielding as summarized in Table A3. A selected set of modulation functions from these measurements are shown in Figures 4.2 and 4.3. The modulation functions in these figures are shown for 2 gamma ray energy regions: DAQ channel numbers 0 - 300 (corresponding to photon energies of approximately 0 - 500 keV) and DAQ channel numbers 300 - 1000 (corresponding to photon energies of approximately 500 keV - 2 MeV). The higher energy region includes the photopeaks for both Cs-137 and Co-60, while the lower energy region is dominated by lower energy photons from down-scattering in the scintillation detectors, RMC masks and structure or in the source shielding and environment. The modulation functions show the counts per second detected by each of the three detectors as a function of mask rotation angle.

The parameters of the gamma imager are summarised in Appendix A and in Table A1. Figures A1 to A3 show the experimental setup. Figure 4.2 shows the modulation signals originating from a Co-60 radiation source located on the rotation axis of the gamma imager. For a single detector RMC this would be a non-modulated blind spot [16].

The gamma imager was used to measure a Cs-137 (33.8 GBq) source through a 0.5 m thick brick wall that is part of the DSTO radiological laboratory. The laboratory was specifically designed to have such wall thickness to ensure that most of the radiation would be absorbed by the wall. Figure 4.3 shows data collected by the gamma imager. A clear modulation of the signal can be observed and the source position was reconstructed accurately.

# 5 Image reconstruction

The RMC image reconstruction consists of matching a measured modulation signal to a matrix of expected reference modulation signals covering the field of view of the imager. For this work the expected reference functions were generated using a ray tracing simulation program written in the MatLab language. This simulation program contained a representation of the main attenuating objects of the RMC; tungsten bars, aluminium structure and the scintillation detectors. The reference function matrix consisted of approximately 100X100 simulation points in the approximately $40^o$X$40^o$ field of view of the RMCs, matching the expected resolution of the imager. In calculating the attenuation of the simulated signal, a gamma ray energy corresponding to the emission peak of Cs-137 (0.662 MeV) was used.

Image reconstructions were accomplished using an implementation of the Maximum Likelihood Expectation Maximisation (MLEM) algorithm as described in [16]. The MLEM method provides a well known iterative solution to minimisation that is simple and flexible and will converge on at least a local minimum (see for example [17]). Equation 5.1 shows the steps that are taken at each iteration. The efficacy of the MLEM method depends on a number of factors including the accuracy of the reference functions, the number of iterations and the degeneracy inherent in the detector design.

$$\lambda_{n+1} = \lambda_n . A^T [y . \frac{1}{A\lambda_n + b}] . \frac{1}{a} \tag{5.1}$$

where dots represent element wise multiplications, $\lambda$ is a vector of points in the image for each iteration $n$ and $A$ is a 2D matrix representing the expected reference modulation signal at the image point locations in $\lambda$. $A$ has dimensions of the number of image points by the number of measurements made in each RMC mask rotation and $y$ is the measured signal from the RMC. The vector b contains the assumed background values at each angle and

$$a = AI \tag{5.2}$$

where $I$ is a vector of ones.

Given that the RMC version 2 has three detectors the signal $y$ is the concatenation of all three detectors. To account for any non-modulated signal not represented correctly in the reference functions dummy signals were added to the matrix $A$ of unit value for each detector. This also allows the algorithm to fit for the unmodulated background which is generally not independently measured.

Figures 5.1 to 5.4 show source reconstruction results using 1000 iterations ($n$=1000) of equation 5.1. The color contour scales at the side of each image indicate the count rate at the detector for each pixel in the image. In each case where there was a source within the field of view, a clear source location was resolved at the measured source location. Each of the reconstructed locations were to within approximately $0.5^o$ of the measured location of the source during the experiment. Figure 5.5 shows an example of the image reconstruction where no source was present. As can be seen the algorithm will attempt to fit the measured modulation signal even when it contains only noise. The MLEM algorithm also has well known "over-fitting" behaviour where it will continue to add signal from the reference functions to provide a fit that is better than allowable given the underlying Poisson statistics of the gamma count-rate [18]. Work on implementing MLEM stopping and source detection trigger algorithms is continuing and will be reported at a later date.

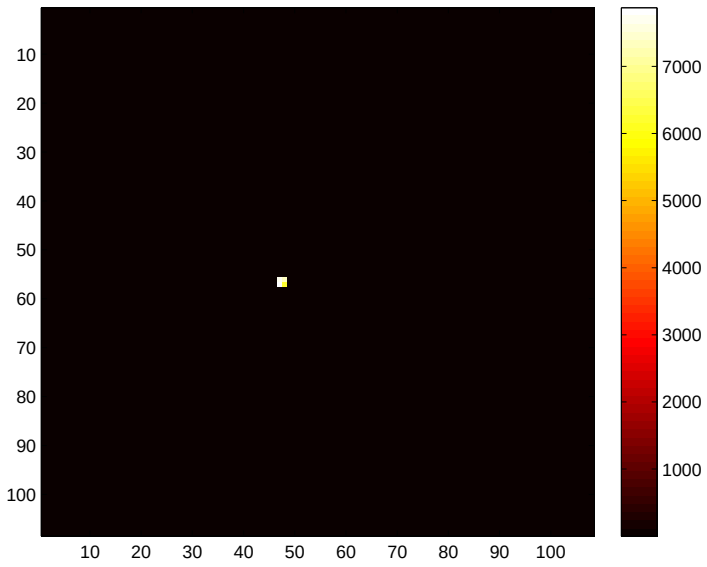


***Figure 5.1:*** *Unshielded Cs-137 (5.02 GBq) source at 7.32 m from the source. Measured x=-0.39 m y=0.13 m, Reconstructed x=-0.34 m y=0.13 m. The x and y axes numbers refer to the pixel location of the reconstruction reference data as described in the text. The side colour bar represents the relative source strength assigned to each pixel as measured at the detector*

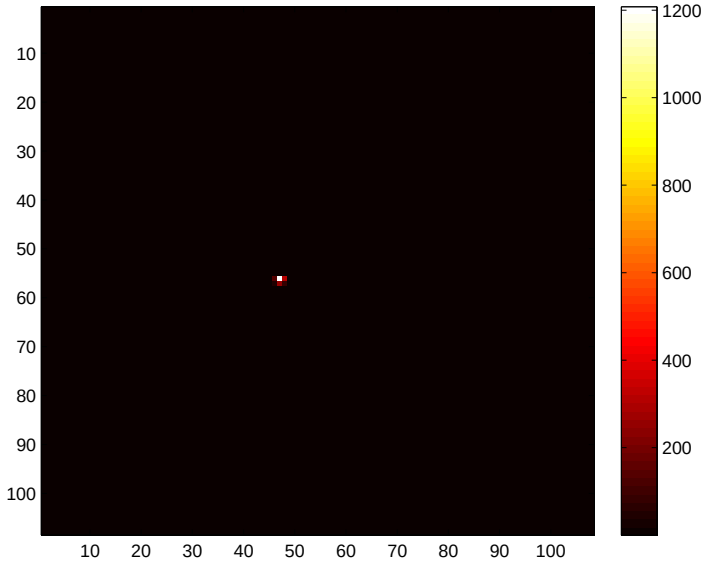


***Figure 5.2:*** *Unshielded Co-60 (0.67 GBq) source at 7.32 m from the source. Measured x=-0.41 m y=0.14 m, Reconstructed x=-0.36 m y=0.10 m. The x and y axes numbers refer to the pixel location of the reconstruction reference data as described in the text. The side colour bar represents the relative source strength assigned to each pixel as measured at the detector*

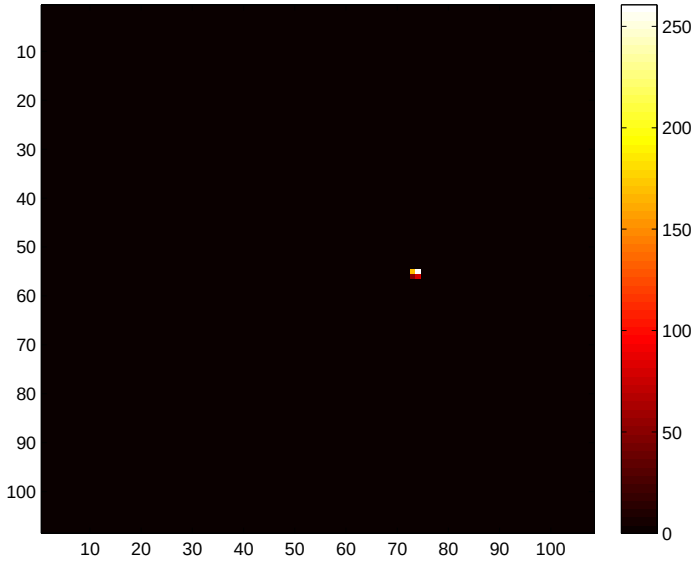


***Figure 5.3:*** *Shielded Cs-137 (33.8 GBq) source in shipping container at 5.82 m from the source. Measured x=0.76 m y=0.09 m, Reconstructed x=0.81 m y=0.04 m. The x and y axes numbers refer to the pixel location of the reconstruction reference data as described in the text. The side colour bar represents the relative source strength assigned to each pixel as measured at the detector*

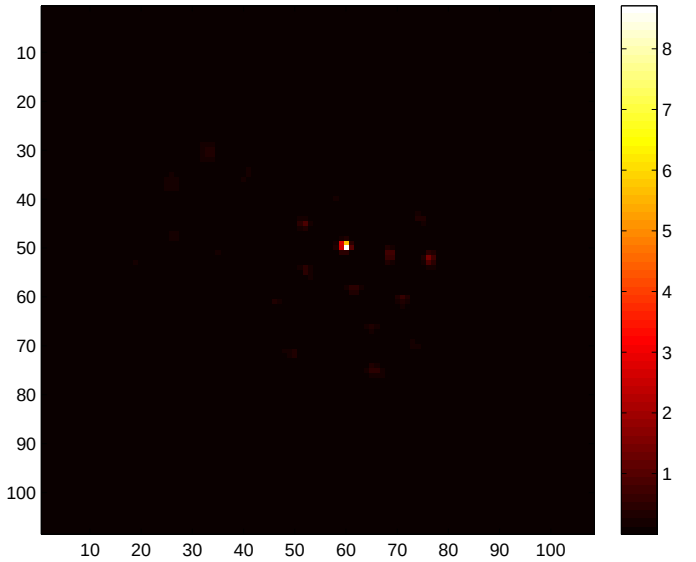


***Figure 5.4:*** *Shielded Co-60 (0.67 GBq) source through the 50 cm brick wall of the radiation laboratory at 3.67 m from the source. Measured x=0.09 m y=-0.18 m, reconstructed x=0.15 m y=-0.11 m. The x and y axes numbers refer to the pixel location of the reconstruction reference data as described in the text. The side colour bar represents the relative source strength assigned to each pixel as measured at the detector*

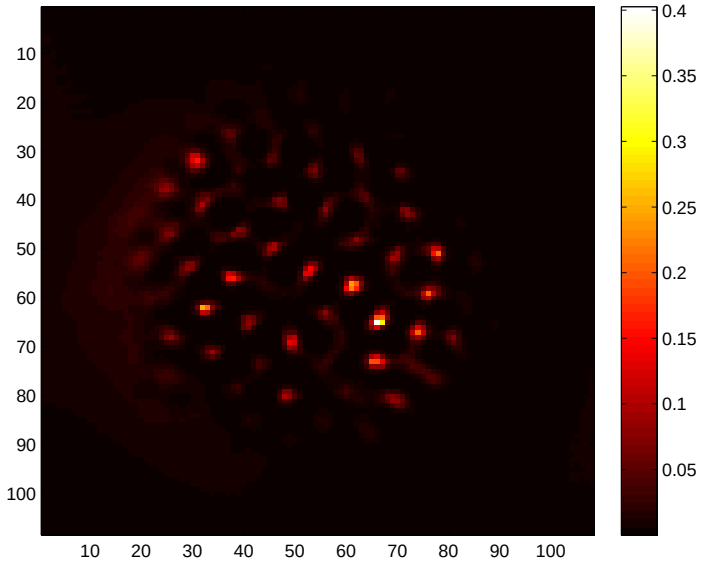


***Figure 5.5:*** *An image taken in the radiation laboratory with no source present*

# 6 Conclusions and further work

The construction and testing of two simple RMC gamma imagers at DSTO has demonstrated that these relatively simple detectors can reliably image gamma sources. The version 1 RMC was very crude, but could still image heavily shielded sources. With only a single 2" NaI detector, though, it had limited sensitivity and a blind area along the mask rotation axis of the device. Due to the limitations of the data acquisition system of the NaI detector it did not produce a gamma spectrum that could be used for isotope identification. The lessons learned from the testing of version 1 were used to design and build a second version RMC with significantly improved capability. The version 2 imager can reliably image heavily shielded sources, including a 0.74 GBq Co-60 source that was imaged through a 0.5 m thick brick wall. It is planned to use the gamma imagers as a test bed for developing a Geant4 based modelling capability in the radiological defence area of DSTO. The prototype imagers will be used in lab and field trials to assess the possible role of gamma imaging in Defence's radiological source search capability. Further prototype imagers are being developed to demonstrate this imaging capability to interested Defence clients.

# References


1. Commercial Radioactive Sources: Surveying the Security Risks, Ferguson C. D., Kazi T. and Perera J., Center for Nonproliferation Studies, Monterey Institute of International Studies, California (2003).

2. Radiation field estimation using a Gaussian mixture, Morelande M. R., Skvortsov A., FUSION '09. 12th International Conference on Information Fusion, pp 2247-2254 (2009).

3. Information Driven Search for Point Sources of Gamma Radiation, Ristic B., Morelande M. R. and Gunatilaka A., Signal Processing, vol. 90, issue 4, pp 1225-1239 (2010).

4. Experimental Verification of Evolutionary Estimation Algorithms for Radioactive Source localisation, Mendis C. et al., $5^{th}$ Int. Conf. Intelligent sensors, sensor networks and Information Processing, ISSNIP09, Melbourne, Australia, December 7-10 (2009).

5. Strategic Review of Radiological Defence Issues - Phase 2, Marinaro D. and Eleftherakis A., DSTO-GD-0592 (2009) [SECRET].

6. Final Report of the CBR MOU International Task Force-53 on Pre-Event Radiological Standoff, Detection [SECRET AS/CA/UK/US EO] (2012).

7. Geant4 developments and applications, Allison J. et al., IEEE Trans. on Nucl. Sci, vol 53, Issue 1 (2006)

8. Coded aperture imaging in X- and Gamma-ray astronomy, Caroli E. et al., Space Sci. Rev., vol. 45, no. 3-4, pp 349-403 (1987).

9. Nuclear Medicine Instrumentation, Prekeges J., Jones & Bartlett Learning; $2^{nd}$ edition (2012).

10. Gamma-Ray Imaging Spectrometry, Science & Technology Review, Lawrence Livermore National Laboratory (1995).

11. Gamma Ray Energy Measurement using the Multiple Compton Technique, Kroeger R. A. et al., IEEE Nuc Sci Symp Conf Record, pp 8/7-8/11 (2000).

12. Single Pinhole and Coded Aperture Collimation Systems for High-Resolution Gamma-Ray Imaging in Nuclear Medicine: a Comparative Study, Fiorini C., Accorsi R. and Lucignani G., IEEE Nuc Sci Symp Conf Record, pp 2938-2941 (2005).

13. A Coded Aperture for High-Resolution Nuclear Medicine Planar Imaging with a Conventional Anger Camera: Experimental Results, Accorsi R,, Gasparini F. and Lanza R. C., IEEE Trans Nuc Sci, vol 48(6), pp 2411-2417 (2001).

14. Rotating Modulation Collimator Imagers, Smith D. M., Hurford G. J. and Boggs S. E., New Astronomy Reviews v48, pp 209-213 (2004).

15. Design and Construction of a Prototype Rotation Modulation Collimator for Near-Field High-Energy Spectroscopic Gamma Imaging, Sharma A. C. et al., 2006 IEEE Nuc Sci Symp Conf Record, pp 2021-2022 (2006).

16. A rotating modulation imager for the orphan source search problem, Kowash R. B., PhD Thesis, University of Michigan (2008).

17. Maximum likelihood reconstruction for emission tomography, Shepp L. A. and Vardi Y., IEEE Trans. Med. Imaging vol MI-1, pp 113-122 (1982).

18. Revisiting stopping rules for iterative methods used in emission tomography, Guo H. and Renaut R. A., Comput Med Imaging Graph. 35(5) pp 398-406 (2011).

# Appendix A Experimental details

Table A1 summarises the parameters of the gamma imager versions 1 and 2.

***Table A1:*** *Gamma imager parameters ( [1]offset: + = left, - = right, when viewing the source from the imager; [2]front mask is further away from the NaI detectors; [3]rear mask is closer to the NaI detectors)*

| Parameter [all in mm] | Imager v1 | Imager v2 |
|---|---|---|
| mask separation (inner side) | 164.00 | 332.00 |
| mask thickness | 12.00 | 19.05 |
| mask diameter | 50.80 | 148.00 |
| slit width | 4.00 | 9.52 |
| slat width | 4.00 | 9.52 |
| bar offset[1] for front mask[2] | 0 | 0 |
| bar offset[1] for rear mask[3] | -2.00 | -4.76 |
| distance between rear mask and detector surface | 2.00 | 7.50 |

Figures A1, A2 and A3 show typical experimental setups used during testing of the RMC imager.

Tables A2 and A3 list the source position, shielding material and source information for experimental data collected for versions 1 and 2 of the imager respectively. The nomenclature of the source position with respect to the centre of the NaI scintillation crystals is shown in Figure A4. The centre position of a single NaI detector crystal (Imager v1) and of three NaI crystals (Imager v2) is assumed to be at a position of $[x,y,z]=[0,0,0]$. The position of the source is indicated by $[x,y,z]=[S_X,S_Y,S_Z]$.

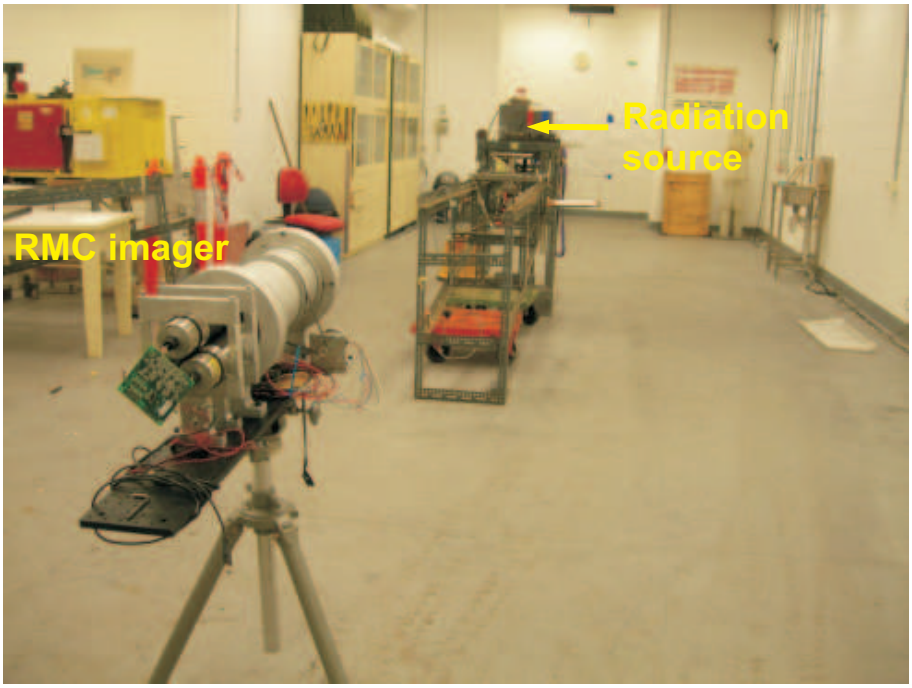


***Figure A1:*** *Experimental setup used to measure unobstructed and shielded radiation sources*

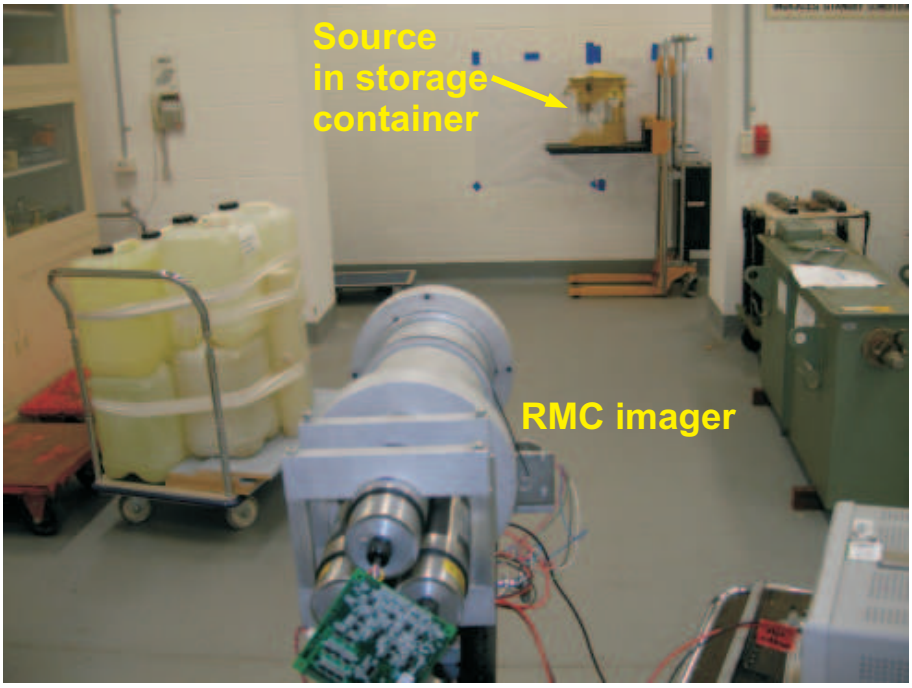


***Figure A2:*** *Experimental setup used to measure radiation source stored in its lead and steel shielding transport container*

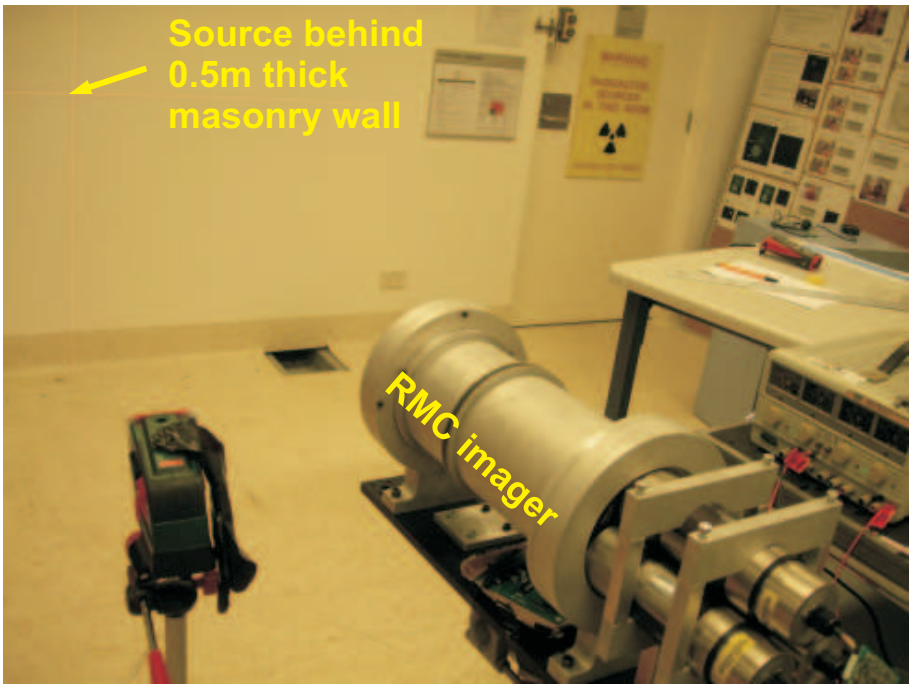


***Figure A3:*** *Experimental setup used to measure a radiation source located behind a* 0.5*m thick masonry wall*

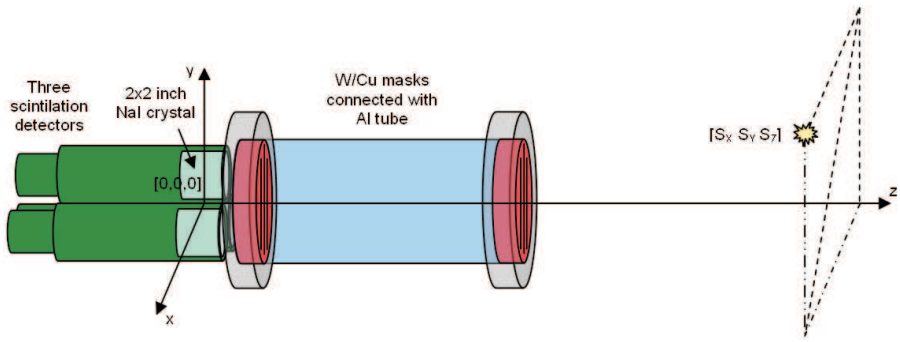


***Figure A4:*** *Nomenclature of the source position with respect to the centre point of the NaI crystals (shown for RMC version 2)*

***Table A2:*** *RMC version 1 - source and shielding data used in experiments ('*' indicates data shown within this report)*

| Source | Source activity | Shielding | $[S_X,S_Y,S_Z]$ $[mm]$ |
|---|---|---|---|
| *Cs-137 | 34.47 GBq | Lead 59mm (storage container) | (-160, -150, 3045.4) |
| Cs-137 | 5.12 GBq | Lead 59mm (storage container) | (-85,-190,2075.4) |
| Co-60 | 0.74 GBq | Lead 59mm (storage container) | (-167,-150,3105.4) |
| Cs-137 | 5.12 GBq | - | (-280, -143, 4195.4) |
| Cs-137 | 5.12 GBq | Metal 10mm | (-280, -143, 4195.4) |
| Cs-137 | 5.12 GBq | Lead 3.6mm | (-280, -143, 4195.4) |
| Cs-137 | 5.12 GBq | Lead 44mm | (-280, -143, 4195.4) |
| Cs-137 | 5.12 GBq | Wood 194mm | (-280, -143, 4195.4) |
| Cs-137 | 5.12 GBq | Concrete bricks 123mm | (-280, -143, 4195.4) |
| Cs-137 | 5.12 GBq | - | (-305, -120, 5195.4) |
| Cs-137 | 5.12 GBq | Metal 10mm | (-305, -120, 5195.4) |
| Cs-137 | 5.12 GBq | Lead 3.6mm | (-305, -120, 5195.4) |
| Cs-137 | 5.12 GBq | Lead 44mm | (-305, -120, 5195.4) |
| Cs-137 | 5.12 GBq | Wood 194mm | (-305, -120, 5195.4) |
| Cs-137 | 5.12 GBq | Concrete bricks 123mm | (-305, -120, 5195.4) |
| *Co-60 | 0.74 GBq | - | (-138, -328, 5203.4) |
| Co-60 | 0.74 GBq | - | (-138, -328, 5203.4) |
| Co-60 | 0.74 GBq | Metal 10mm | (-138, -328, 5203.4) |
| Co-60 | 0.74 GBq | Lead 3.6mm | (-138, -328, 5203.4) |
| *Co-60 | 0.74 GBq | Lead 44mm | (-138, -328, 5203.4) |
| Co-60 | 0.74 GBq | Wood 194mm | (-138, -328, 5203.4) |
| Co-60 | 0.74 GBq | Concrete bricks 123mm | (-138, -328, 5203.4) |
| Cs-137 | 512 GBq | - | (-1596, -157, 16625.4) |
| Co-60 | 0.74 GBq | - | (1760, -548, 16625.4) |
| Cs-137 | 5.12 GBq | Brick wall 0.5m | (225, 204, 2500) |
| Co-60 | 0.74 GBq | Brick wall 0.5m | (363, -396, 3025.4) |
| Co-60 | 0.74 GBq | Brick wall 0.5m | (-288, -210, 3945.4) |

***Table A3:*** *RMC version 2 - source and shielding data used in experiments ('*' indicates data shown within this report)*

| Source | Source activity | Shielding | $[S_X,S_Y,S_Z]$ $[mm]$ |
|---|---|---|---|
| Cs-137 | 33.8 GBq | Lead 59mm (storage container) | (-700, -780, 5508) |
| *Cs-137 | 33.8 GBq | Lead 59mm (storage container) | (757, 90, 5823) |
| Cs-137 | 33.8 GBq | Lead 59mm (storage container) | (0, 0, 5847) |
| Co-60 | 0.67 GBq | Lead 59mm (storage container) | (725, -79, 4980) |
| *Cs-137 | 5.02 GBq | - | (-390, 133, 7323) |
| *Co-60 | 0.67 GBq | - | (-415, 136, 7323) |
| Co-60 | 0.67 GBq | Lead 44mm | (-415, 136, 7323) |
| Co-60 | 0.67 GBq | Concrete bricks 123mm | (-415, 136, 7323) |
| *Co-60 | 0.67 GBq | - | (0, 0, 7323) |
| Co-60 | 0.67 GBq | Brick wall 0.5m | (90, -180, 3673) |
| *Cs-137 | 33.8 GBq | Brick wall 0.5m | (-406, -180, 3673) |

| **DEFENCE SCIENCE AND TECHNOLOGY ORGANISATION DOCUMENT CONTROL DATA** | 1. CAVEAT/PRIVACY MARKING |
|---|---|

| 2. TITLE | 3. SECURITY CLASSIFICATION |
|---|---|
| Gamma Imaging using Rotational Modulation Collimation | Document (U)<br>Title (U)<br>Abstract (U) |
| 4. AUTHORS | 5. CORPORATE AUTHOR |
| M. Roberts M. Kocan, A. Eleftherakis, D. Marinaro and A. Meehan | Defence Science and Technology Organisation<br>506 Lorimer St,<br>Fishermans Bend, Victoria 3207, Australia |

| 6a. DSTO NUMBER | 6b. AR NUMBER | 6c. TYPE OF REPORT | 7. DOCUMENT DATE |
|---|---|---|---|
| DSTO–TR–2946 | 015-881 | Technical Report | January 2014 |

| 8. FILE NUMBER | 9. TASK NUMBER | 10. TASK SPONSOR | 11. No. OF PAGES | 12. No. OF REFS |
|---|---|---|---|---|
| 2013/1156274 | 07/079 | CO-SOER | 15 | 18 |

| 13. URL OF ELECTRONIC VERSION | 14. RELEASE AUTHORITY |
|---|---|
| `http://www.dsto.defence.gov.au/publications/scientific.php` | Chief, Land Division |

15. SECONDARY RELEASE STATEMENT OF THIS DOCUMENT

*Approved for Public Release*

OVERSEAS ENQUIRIES OUTSIDE STATED LIMITATIONS SHOULD BE REFERRED THROUGH DOCUMENT EXCHANGE, PO BOX 1500, EDINBURGH, SOUTH AUSTRALIA 5111

16. DELIBERATE ANNOUNCEMENT

No Limitations

17. CITATION IN OTHER DOCUMENTS

No Limitations

18. DSTO RESEARCH LIBRARY THESAURUS

radiation, radiological defence, radiation detection

19. ABSTRACT

This report describes measurements undertaken at the DSTO radiation laboratory to characterise the performance of two rotating modulation collimator (RMC) gamma imagers built by DSTO. The ability of these devices to image shielded and unshielded Co-60 and Cs-137 sources is demonstrated. A discussion of the characteristics of this and other gamma imaging techniques and their application in a Defence context is included.